Journal of the Geological Society

Clinopyroxene–rutile phyllonites from the East Tenda Shear Zone (Alpine Corsica, France): pressure–temperature–time constraints to the Alpine reworking of Variscan Corsica

Matteo Maggi, Federico Rossetti, Fernando Corfu, Thomas Theye, Torgeir B. Andersen and Claudio Faccenna

Journal of the Geological Society 2012, v.169; p723-732.
doi: 10.1144/jgs2011-120

Notes

Journal of the Geological Society, London, Vol. **169**, 2012, pp. 723–732. doi: 10.1144/jgs2011-120.

Clinopyroxene–rutile phyllonites from the East Tenda Shear Zone (Alpine Corsica, France): pressure–temperature–time constraints to the Alpine reworking of Variscan Corsica

MATTEO MAGGI[1], FEDERICO ROSSETTI[1*], FERNANDO CORFU[2], THOMAS THEYE[3], TORGEIR B. ANDERSEN[2] & CLAUDIO FACCENNA[1]

[1]*Dipartimento di Scienze Geologiche, Università Roma Tre, Roma, Italy*

[2]*Department of Geosciences, Oslo University, Oslo, Norway*

[3]*Institut für Mineralogie und Kristallchemie, Universität Stuttgart, Stuttgart, Germany*

**Corresponding author (e-mail: rossetti@uniroma3.it)*

Abstract: The East Tenda Shear Zone is the regional structure that marks the Alpine overthrusting of the Ligurian–Piedmontese ocean onto the Variscan Corsica. We present the first report of a Na-pyroxene (acmite)–rutile-bearing assemblage from a phyllonitic shear zone that occurs within the gneissic lithologies of the East Tenda Shear Zone. Acmite hosts inclusions of Na-amphibole and titanite, and is rimmed by retrogressive biotite. Forward modelling of the shear zone assemblages in the NCKFMASTHO chemical system indicates a cold burial–exhumation path (palaeogeothermal gradient <10 °C km^{-1}) and a metamorphic climax with minimum pressure of 1.2 GPa and temperatures of 350–400 °C. U–Pb thermal ionization mass spectrometry analyses on synkinematic rutile yield a 3D array with an age of 48 ± 18 Ma (MSWD 7.3), whereas coexisting acmite–phengite and coatings of oxides or sulphides provide an intercept at 54 ± 8 Ma (MSWD = 48). The scatter of the arrays is considered to reflect secondary disturbances of the system and the age provided by acmite–phengite and the coatings at 54 ± 8 Ma is considered the most reliable estimate for shear zone formation. Implications of these new metamorphic and geochronological data are discussed in the regional framework of the Alpine geology and integrated in the plate-tectonic scenario of the central Mediterranean.

Shear zones in the middle and lower crust exert an important control on the metamorphic processes and tectonic reworking in orogenic belts (e.g. Austrheim 1987; Selverstone *et al*. 1991; Imber *et al*. 1997; Jolivet *et al*. 2005). The systematic spatial association between zones of ductile deformation and zones of fluid infiltration has led many researchers to suggest that deformation, fluid flow, metamorphic reactions and changes in the bulk rheology are mutually reinforcing processes (e.g. Austrheim 1987; Dipple & Ferry 1992; Jolivet *et al*. 2005; John *et al*. 2009). Furthermore, enhanced fluid–rock interaction in shear zones may cause major changes in mineralogy and bulk-rock chemistry via metasomatism, including the resetting of radiogenic as well as stable isotopes (e.g. Selverstone *et al*. 1991; Clark *et al*. 2005). Such pervasive changes are useful for determining the conditions and timing of deformation, which otherwise may be subtle and barely detectable in the unreacted rock mass. This is particularly relevant at depth within continental basement complexes reactivated during orogenic events, as granitoids and high-grade metamorphic or other mostly 'dry' rocks are the dominant lithology (e.g. Labrousse *et al*. 2010).

In this paper we present new petrological and geochronological data from the East Tenda Shear Zone of Alpine Corsica (Fig. 1). This shear zone is the deformation zone that marks the Alpine overthrusting of the Ligurian–Piedmontese oceanic domain (Schistes Lustrés unit) onto the basement rocks of the Variscan Corsica (see Gueydan *et al*. 2003; Molli & Malavieille 2010; Fig. 1b). Despite the regional significance, the pressure–temperature–time (*P–T–t*) evolution of this shear zone is still poorly constrained, particularly concerning the timing of the Alpine metamorphic climax. We report the first occurrence of clinopyroxene (acmite)–rutile assemblages from the East Tenda Shear Zone and fix the time of the Alpine high-pressure stage in the Early Eocene (54 ± 8 Ma) by U–Pb isotope dilution thermal ionization mass spectrometry (ID-TIMS) dating of the synkinematic assemblage. The implications of these new metamorphic and geochronological data, which are coupled to fabric development within the East Tenda Shear Zone, are discussed in the regional framework of the Alpine geology of the central Mediterranean.

Regional geological setting

The island of Corsica is located in the centre of the western Mediterranean, between the Liguro-Provençal and Tyrrhenian back-arc basins (Fig. 1a). The island consists mostly of a variably deformed Variscan crystalline basement with a Permian–Eocene sedimentary cover, which constituted part of the European foreland domain of the Alpine orogeny (e.g. Rossi *et al*. 2003; Malasoma & Marroni 2007). Alpine Corsica forms the northeastern parts of the island, and is made up of a nappe stack largely composed of ophiolitic rocks with associated (meta)-sedimentary cover and slivers of continental basement, composed of rocks originally formed within the Neotethyan Ligurian–Piedmontese oceanic basin and along the Tethyan ocean–continent transition (see Vitale Bravarone *et al*. 2011*a*; Fig. 1b). The structural architecture of Alpine Corsica consists of a lower nappe system (the Schistes Lustrés nappe) affected by subduction zone metamorphism and an upper, low-grade metamorphosed nappe complex comprising the Balagne, Nebbio and Macinaggio units (e.g. Mattauer *et al*. 1981; Dallan & Nardi 1984; Durand-Delga 1984; Waters 1990; Fournier *et al*. 1991; Dallan & Pulcinelli 1995; Daniel *et al*. 1996; Malavieille *et al*. 1998; Rossi *et al*. 2003; Molli & Malavieille 2010). During the Alpine orogeny the continental European basement, the ophiolitic rocks of the Ligurian–Piedmontese basin and their deep-marine sedimentary

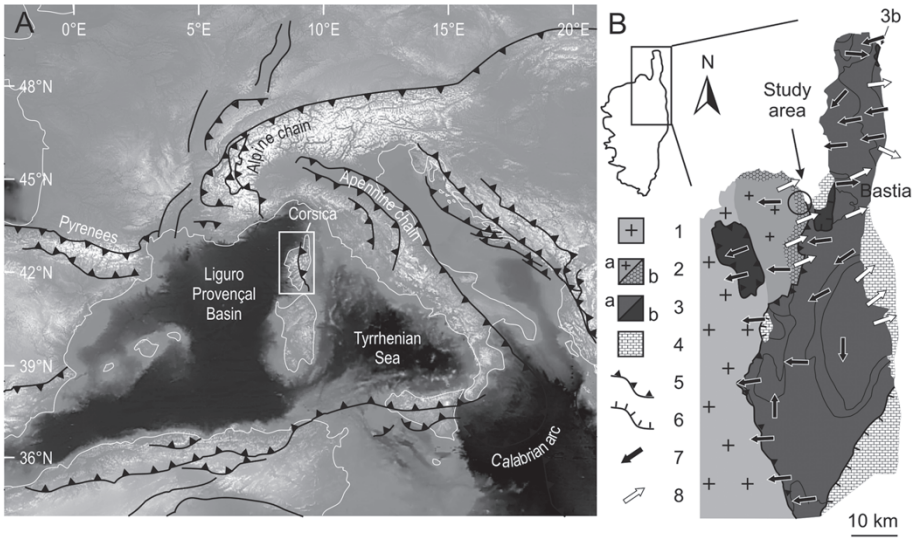

Fig. 1. (**a**) Digital elevation model of the western Mediterranean region with the main tectonic boundaries indicated (modified after Jolivet *et al*. 1998). The white rectangle indicates the position of Corsica. (**b**) Synthetic structural–geological map of Alpine Corsica (modified after Daniel *et al*. 1996; Molli & Malavieille 2010, and reference therein). 1, Hercynian basement; 2a, Tenda unit; 2b, East Tenda Shear Zone (ETSZ); 3, Ocean-derived units (a, Schistes Lustrés units; b, Balagne, Nebbio and Macinaggio units); 4, Miocene and Quaternary deposits; 5, main thrusts; 6, main extensional faults and detachments; 7, D_1 sense of shear; 8, D_2 sense of shear.

cover were affected by the subduction-related blueschist- to eclogite- and lawsonite-eclogite-facies metamorphism (e.g. Essene 1968; Caron *et al*. 1981; Lahondère & Guerrot 1997; Tribuzio & Giacomini 2002; Chopin *et al*. 2008; Ravna *et al*. 2010; Vitale Brovarone *et al*. 2011*a*, *b*).

The transition between the Variscan and the Alpine domains occurs along the Tenda Massif, in a deformation zone that formerly constituted the extended continental margin of the European basement (see Molli & Malavieille 2010), known as the East Tenda Shear Zone. This portion of the Variscan crust was strongly reworked during the Alpine orogeny, synkinematically with epidote- to blueschist-facies metamorphism (Gibbons & Horak 1984; Daniel *et al*. 1996; Tribuzio & Giacomini 2002; Gueydan *et al*. 2003; Molli *et al*. 2006). The fabrics of the East Tenda Shear Zone are composite, recording both the overthrusting and the subsequent exhumation of the Schistes Lustrés nappe. Contrasting kinematic and tectonic interpretations have previously been proposed to explain these fabrics. Molli *et al*. (2006) emphasized the top-to-the-west compressional shearing as the dominant structural grain in the East Tenda Shear Zone, whereas others considered top-to-the-east ductile-to-brittle extensional reactivation along the contact with the Schistes Lustrés to be the dominant fabric (Jolivet *et al*. 1990; Gueydan *et al*. 2003; Daniel *et al*. 1996).

The age of the HP–LT Alpine deformation and metamorphism in Corsica is still poorly constrained (see recent summary by Martin *et al*. 2011). The earliest and coldest metamorphic stage, which produced lawsonite-bearing eclogites near the 'forbidden zone' in parts of the Schistes Lustrés units (Ravna *et al*. 2010; Vitale Bravarone *et al*. 2011*b*) is believed to be late Cretaceous (e.g. Molli & Malavieille 2010, and references therein), based on the available Sm–Nd whole-rock (garnet–glaucophane–clinopyroxene) isochron age of 84 ± 5 Ma (Lahondère & Guerrot 1997) and the *c*. 90 Ma $^{40}Ar/^{39}Ar$ glaucophane ages (Maluski 1977) from eclogite lenses within the Schistes Lustrés. Lawsonite eclogites were synkinematically decompressed at both blueschist and later greenschist facies, and have therefore experienced a protracted structural and metamorphic history. Recent U–Pb zircon ages from continental-derived granulite slivers found within the Schistés Lustres gave an age of 34.4 ± 0.8 Ma that is considered to date the Alpine pressure peak during reactive fluid infiltration in Alpine Corsica (Martin *et al*. 2011). This Tertiary age is in line with the biostratigraphic constraints provided by the nummulite-bearing sedimentary sequences of the Alpine foreland involved in the Alpine nappe construction, which suggests a post Middle Eocene orogenic construction and metamorphism at the expense of the Corsica–Europe continental margin (Bezert & Caby 1988; Egal 1992; Brunet *et al*. 2000; Malasoma & Marroni 2007). In the Schistes Lustrés, Tertiary metamorphic ages are provided by $^{40}Ar/^{39}Ar$ geochronology (Maluski 1977; Amaudric Du Chaffaut & Saliot 1979; Brunet *et al*. 2000). In particular, discordant $^{40}Ar/^{39}Ar$ phengite ages ranging from 65 to 55 Ma and from 55 to 37 Ma are derived from eclogite and blueschist units, respectively (Brunet *et al*. 2000). In the East Tenda Shear Zone, $^{40}Ar/^{39}Ar$ phengite dating provided ages between 45 and 30 Ma (Brunet *et al*. 2000), whereas earlier Rb–Sr whole-rock data point to a Middle Cretaceous (108 ± 5 Ma) age (Cohen *et al*. 1981).

Structures and petrography

Deformation is heterogeneously distributed within the East Tenda Shear Zone, with zones of localized ductile-to-brittle shearing (SZ) that wrap around lens-shaped massive lenses (ML) with a prominent gneissic texture (Figs 2 and 3a). The main foliations in the East Tenda Shear Zone and the overlying Schistes Lustrés are nearly concordant and strike NW–SE and dominantly dip shallowly towards the NE (Fig. 2). In the following, mineral abbreviations follow Whitney & Evans (2010).

The mineralogy of the ML consists of a high-variance assemblage of Qz, Ph and relic igneous Fsp with Ep, Fe-oxides, relic Zrn and Aln as accessory phases. The SZ mineralogy is invariably dominated (40–60 vol%) by highly substituted Ph (Si^{4+} = 3.5–3.7 a.p.f.u.), modally abundant Qz (30–50 vol%), Ab (10–20 vol%), Ep (5–10 vol%) and Mc (5–10 vol%). Locally, Na-Amp (10–20 vol%) also occurs in the SZ assemblage to form mostly thin (up to 0.5 m thick) dark bluish mylonitic layers (Fig. 3a and b). Stretching lineations trend WSW–ENE to east–west (Fig. 2) and are provided by aggregates of Qz–Ph–Ab in the ML and of Qz–Ph–Ab ± Na-Amp in the SZ. Kinematic indicators, at outcrop and thin-section scale, systematically indicate top-to-the-west ductile shear sense in both ML and SZ (Fig. 3b and c). Semi-brittle to brittle top-to-the-east shear bands locally reactivate the main top-to-the-west ductile shear fabrics. This late deformation is mostly localized within the phyllonitic shear zones (Fig. 3d).

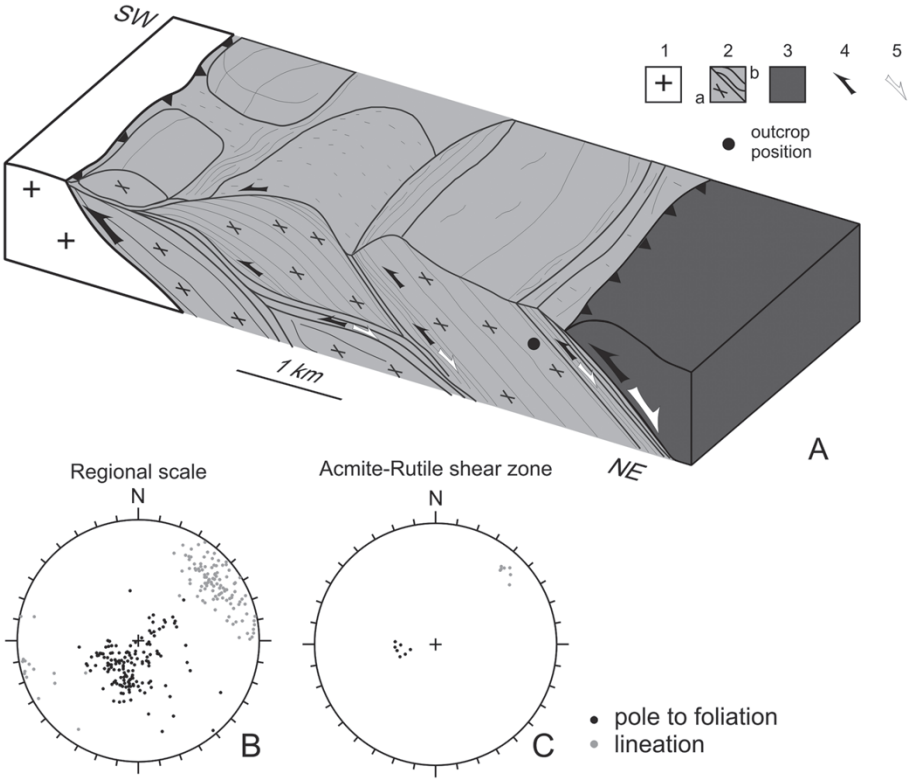

Fig. 2. (**a**) Schematic 3D interpretative block diagram to illustrate the structural architecture and shear fabric within the East Tenda Shear Zone. Shear strain partitioning occurs within this shear zone, with low-strain domains corresponding to the gneissic (massive) lenses wrapped by high-strain domains consisting of mylonitic to phyllonitic shear zones. The kinematics relative to the main compressional fabric development (D_1) and the later extensional reactivation (D_2) are also indicated. 1, protolith rocks; 2, East Tenda Shear Zone units (2a, massive lenses; 2b, shear zones); 3, Schistes Lustrés units; 4, compressional shear senses; 5, extensional shear reactivation. (**b**, **c**) Representative stereoplots (Schmidt net, lower hemisphere projection) showing the plano-linear shear fabrics at regional (**b**) and outcrop (**c**) scale.

Approximately 200 m structurally below the main contact with the Schistes Lustrés (i.e. normal to the main foliation), a 10 cm thick, discontinuous clinopyroxene (acmite)–rutile (Cpx–Rt) phyllonitic shear zone was found, in sharp contact with the host ML (Fig. 3g and f; geographical coordinates 42°39′23.34″N, 9°16′20.74″E). Stretching lineations are provided by Ph–Qz–Cpx–Rt aggregates ± Fsp (Fig. 3g). The modal composition of the phyllonite consists of Ph (>60 vol%), Cpx (20–25 vol%), Qz (2–5 vol%), Rt (2–5 vol%) and alkaline Fsp (Ab and Mc) + Ep + relic Zrc (<5 vol%) as minor phases (Fig. 4a). The Cpx crystals host inclusions of Na-Amp and Ttn and are rimmed by retrogressive Bt; Rt forms porphyroblasts along the main phyllonitic foliation (Fig. 4b and c). Microprobe data and back-scattered electron (BSE) images indicate a rather homogeneous composition both for the Ph (3.6–3.7 Si^{4+} a.p.f.u.) and Cpx (average composition $Acm_{72}Jd_{17}Di_9Hed_1Opx_{0.05}$) (Table 1; Fig. 5). In contrast, Ph in the host rocks shows a strong core-to-rim zonation (Si^{4+} content ranging from 3.3 a.p.f.u. in the core to 3.6 a.p.f.u. in the rim) (Table 1; Figs 4d and 5a). The phengite compositions of rims and in the Cpx–Rt shear zone significantly deviate from the ideal Tschermak's substitution line, suggesting that some of the iron is ferric (Fig. 5a).

Thermobarometry of the Cpx–Rt shear zone

Because of the high-variance shear zone assemblage (Ph–Cpx–Rt–Qz ± Fsp (Ab and Mc) ± Ep), the inverse (conventional and multi-equilibrium) thermobarometry is not applicable. Accordingly, we adopted a forward modelling technique to infer the pressure–temperature (*P–T*) conditions of formation of the Cpx–Rt shear zone. The *P–T–X* modelling was computed using the Perple_X_07 software (Connolly 2005; http://www.perplex.ethz.ch/) in the NKFMASHTO (Na_2O–K_2O–FeO–MgO–Al_2O_3–SiO_2–H_2O–TiO_2–O_2) chemical system, for bulk-rock compositions as calculated from mineral modal compositions and electron microprobe data. We used the thermodynamics dataset of Holland & Powell (1998; updated in 2002) for minerals and aqueous fluids, integrated with those of Massonne & Willner (2008) for low-grade metamorphic Fe^{3+}-bearing phases (Cpx and Na-Amp). In particular, the following solution models offered by Perple_X_07 were chosen: Bio(HP) for Bt, Chl(HP) for Chl, Ep(HP) for Ep, GlTrTsMr for Na-Amp, Acm(M) for Cpx, Gt(HP) for Grt, and fsp11 for Fsp. Water content was considered to be always in excess.

A representative pseudosection is shown in Figure 6. The synkinematic Rt–Cpx–Ph–Qz ± Na-Amp assemblage occurs in a narrow divariant field with minimum pressure of 1.1–1.2 GPa and temperature between 350 and 400 °C. The Si^{4+} isopleths for Ph were calculated to derive a possible *P–T* path. Metamorphic climax is not well constrained. Nevertheless, the presence of Cpx and Rt (and not Ab or Ttn; for pressure) and the absence either of Lws or Bt (for temperature) indicate minimum peak *P–T* conditions for the shear zone development at 1.1–1.2 GPa and *c*. 400 °C.

To constrain the *P–T* path of the East Tenda Shear Zone, the following points should be taken into account: (1) the systematic rimward increase of Si^{4+} in Ph (from 3.3 to 3.6 a.p.f.u.) from the gneissic host rocks; (2) the Na-amph inclusion in Cpx; (3) the only minor core-to-rim variation of Si^{4+} a.p.f.u. in Ph from the Cpx–Rt shear zone. Points (1) and (2) indicate a prograde increase in pressure, whereas point (3) suggests maintenance of highly substituted phengite compositions during exhumation of the East Tenda Shear Zone (Fig. 6). We then propose that the Alpine reworking of the Variscan basement along the East Tenda Shear Zone occurred under a cold (<10 °C km^{-1}) geothermal gradient during a clockwise burial–exhumation path, nearly parallel to the phengite isopleths after achievement of the metamorphic peak (Fig. 6).

The results described above are affected by some degree of uncertainty, mainly owing to the following: (1) representativeness

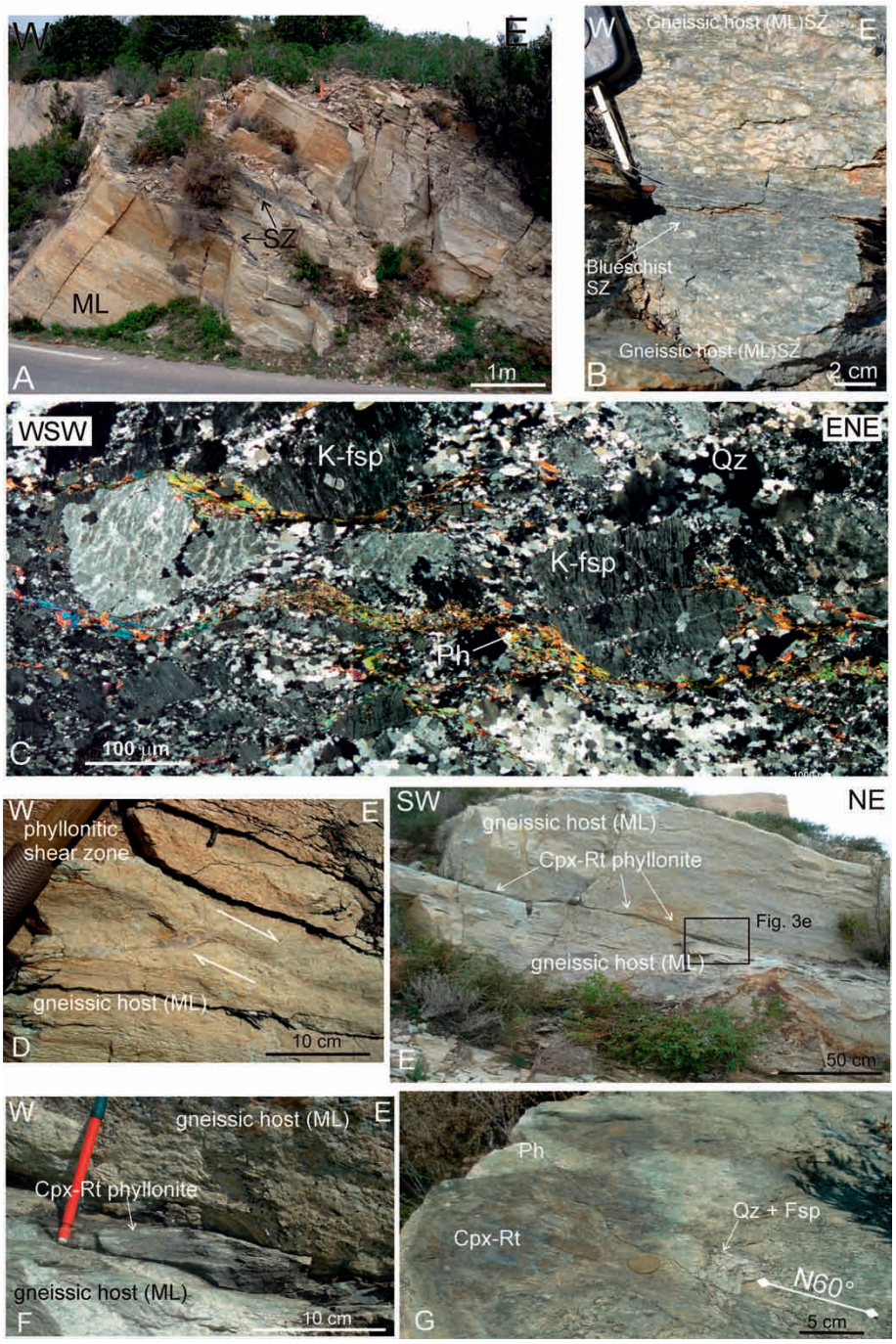

Fig. 3. (**a**) Discrete, blueschist-facies mylonites (phyllonites) cutting across gneissic bodies along the East Tenda Shear Zone. (**b**) A detail of the gneiss–blueschist mylonite transition at the outcrop scale. The pronounced grain-size reduction on entering the shear zone should be noted. Shear sense sinistral (top-to-the-west) as primarily provided by the overall S-C fabric and σ-type quartz and feldspar porphyroclasts in the gneissic host rocks (exposure normal to foliation and parallel to stretching direction). (**c**) Thin section of the gneissic host rocks (section normal to foliation and parallel to stretching lineation; crossed polars). Relic σ-shaped K-feldspar porphyroclasts are embedded in a fine-grained recrystallized quartz–phengite shear matrix. Shear sense sinistral (top-to-the-WNW) as indicated by oblique foliation, mica fish and σ-type feldspar porphyroclasts. (**d**) Semi-brittle, top-to-the-east shearing that reworks the early top-to-the-west mylonitic shear fabrics of the East Tenda Shear Zone. (**e**) The acmite–rutile (Cpx–Rt) phyllonite in the field. The sharp boundaries of the shear zone with the massive gneissic host rocks should be noted. (**f**) Detail of (**e**), showing the shear zone–host rock transition marked by the progressive grain-size reduction and increase of the phengite content. (**g**) Plane view of the acmite–rutile shear zone showing well-developed stretching lineations as provided by the Cpx–Rt–Qz–Fsp assemblage. Mineral abbreviations follow Whitney & Evans (2010).

of the used bulk composition, particularly of the O_2 content; (2) variation of the bulk-rock composition induced by fluid–rock interaction during progressive shearing; (3) significant uncertainty of the thermodynamic dataset in the low *T* range. Accordingly, forward modelling of the Cpx–Rt shear zone can be considered as tentative only and *P–T* estimates as semi-quantitative. Nevertheless, trial calculations with variations of O_2 content, as well as using different bulk compositions, did not result in significant modification of the general aspects of the derived *P–T* path, which was dominantly constrained by the positive slope of the Ph isopleths in the *P–T* interval of interest. In addition, the obtained results are compatible with the previous *P–T* estimates on the Alpine metamorphic climax along the East Tenda Shear Zone, which collectively document epidote- to blueschist-facies peak metamorphism (Tribuzio & Giacomini 2002; Molli *et al*. 2006)

TIMS U–Pb geochronology

To establish the age of shearing along the East Tenda Shear Zone, we analysed Rt and coexisting Cpx, Ph, and oxide or sulphide coatings on Qz. The minerals used for analysis were extracted from the schist by crushing, pulverizing and enrichment on a Wilfley table, and by using magnetic separators and heavy liquid. The selected minerals were dissolved in concentrated HF (+ HNO_3); the Rt in

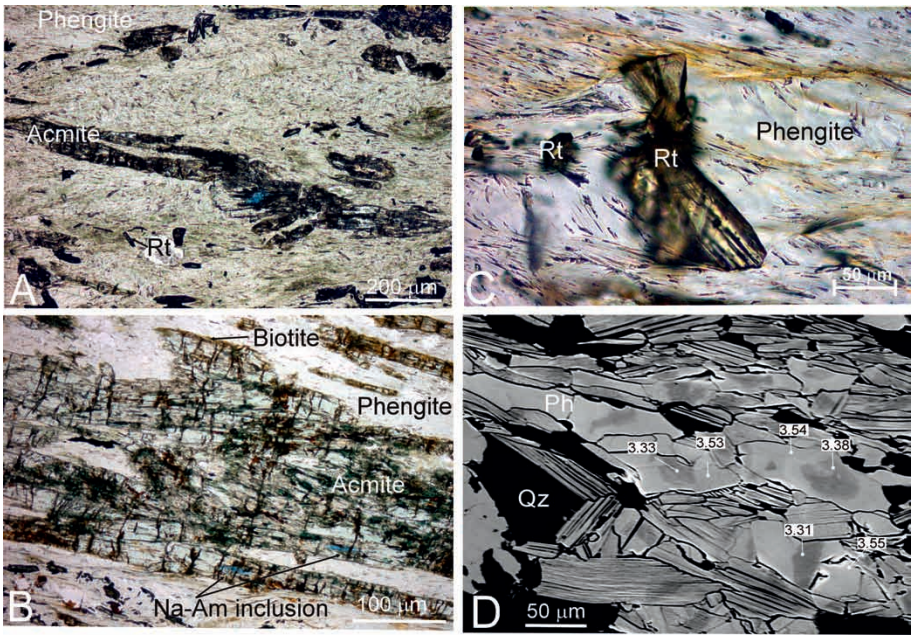

Fig. 4. (**a**) Thin section of the acmite–rutile (Cpx–Rt) shear zone showing Cpx and Rt neoblasts embedded in a microcrystalline phengite (Ph) matrix (plane-polarized light). (**b**) Thin section showing porphyroblastic Cpx hosting inclusions of Na-Amp, rimmed by retrogressive biotite (plane-polarized light). (**c**) Porphyroblastic Rt in the rock matrix (plane-polarized light). (**d**) BSE image of the gneissic host rock showing Ph zoning as documented by the Si^{4+} a.p.f.u. content.

Table 1. *Representative mineral compositions of the Cpx–Rt shear zone samples*

Mineral:	Phengite						Clinopyroxene				Biotite				Na-amphibole (inclusion in Cpx)			
Sample:	Host rock				Cpx–Rt shear zone		Cpx–Rt shear zone				Cpx–Rt shear zone				Cpx–Rt shear zone			
	core	rim	core	rim														
Analysis:	1	3	5	7	15	19		1	4	10		6	13	17		20	14	19
SiO_2	49.48	50.20	49.85	50.72	51.88	55.13	SiO_2	54.29	54.04	52.91	SiO_2	37.18	37.02	37.77	SiO_2	55.11	55.63	55.34
TiO_2	0.09	0.53	0.03	0.62	0.53	0.22	TiO_2	0.77	0.30	0.10	TiO_2	1.70	0.80	0.57	TiO_2	0.06	0.06	0.15
Al_2O_3	27.83	23.51	27.99	22.19	19.00	18.43	Al_2O_3	5.07	5.64	2.64	Al_2O_3	12.50	11.86	10.94	Al_2O_3	2.27	2.31	2.28
FeO_{tot}	3.87	6.33	3.48	6.02	6.28	4.57	FeO_{tot}	22.18	20.51	27.34	FeO_{tot}	31.58	33.00	34.37	FeO_{tot}	22.47	21.03	22.28
MnO	0.24	0.12	0.23	0.17	bdl	0.04	MnO	0.01	0.05	0.02	MnO	0.15	0.12	0.08	MnO	0.12	0.12	0.15
MgO	1.85	2.49	1.96	2.42	5.18	6.62	MgO	1.70	2.22	0.43	MgO	2.72	3.40	1.56	MgO	8.63	9.40	8.60
CaO	bdl	bdl	bdl	0.01	0.03	0.00	CaO	2.54	3.12	0.56	CaO	0.02	bdl	Bdl	CaO	0.36	0.28	0.39
Na_2O	0.01	0.06	0.01	0.26	0.25	0.03	Na_2O	12.53	12.29	13.28	Na_2O	0.07	0.05	1.00	Na_2O	6.97	7.33	7.09
K_2O	11.71	11.42	11.65	10.41	10.00	11.04	K_2O	bdl	bdl	bdl	K_2O	9.55	9.66	8.47	K_2O	0.28	0.47	0.31
BaO	0.04	0.04	0.01	0.24	0.05	0.04	BaO	bdl	0.02	bdl	BaO	0.03	0.05	0.18	BaO	bdl	bdl	bdl
Total	95.12	94.70	95.21	93.06	93.20	96.11	Total	99.09	98.19	97.28	Total	95.50	95.96	94.94	Total	96.27	96.63	96.59
Si	3.363	3.471	3.372	3.541	3.589	3.698	Si	1.993	1.990	1.997	Si	3.011	3.011	3.114	Si	7.988	7.977	7.991
Ti	0.004	0.027	0.001	0.033	0.028	0.011	Al_T	0.007	0.010	0.003	Al_T	0.989	0.989	0.886	Ti	0.006	0.007	0.017
Al	2.229	1.916	2.231	1.826	3.098	2.914	Al_O	0.213	0.235	0.115	Al_O	0.204	0.148	0.176	Al	0.388	0.390	0.389
Fe^{2+}	0.220	0.366	0.197	0.352	0.237	0.196	Ti	0.021	0.008	0.003	Ti	0.104	0.049	0.035	Fe^{3+}	1.531	1.595	1.526
Mn	0.014	0.007	0.013	0.010	0.000	0.000	Fe^{3+}	0.643	0.632	0.855	Fe^{2+}	2.139	2.245	2.370	Fe^{2+}	1.193	0.927	1.164
Mg	0.188	0.257	0.198	0.252	0.534	0.662	Fe^{2+}	0.038	0.000	0.008	Mn	0.011	0.008	0.006	Mn	0.015	0.015	0.018
Ca	0.000	0.000	0.000	0.001	0.000	0.000	Mn	0.000	0.001	0.001	Mg	0.328	0.413	0.191	Mg	1.865	2.009	1.851
Ba	0.001	0.001	0.000	0.007	0.000	0.000	Mg	0.093	0.122	0.024	Ba	0.001	0.000	0.000	Ca	0.056	0.043	0.060
Na	0.001	0.008	0.001	0.035	0.034	0.004	Ca	0.100	0.123	0.022	Ca	0.003	0.004	0.016	Na	1.959	2.038	1.985
K	1.015	1.007	1.005	0.927	0.882	0.944	Na	0.892	0.877	0.972	Na	0.011	0.008	0.160	K	0.052	0.086	0.057
											K	0.986	1.003	0.891				
							Jd	0.227	0.245	0.118					Gln	0.118	0.128	0.121
							Acm	0.665	0.632	0.855	X_{Mg}	0.133	0.155	0.075	Fe–Gln	0.075	0.059	0.076
							Di	0.071	0.123	0.017					Mg–Rbk	0.480	0.556	0.488
							Hd	0.029	0.000	0.006					Rbk	0.3069	0.2566	0.3070
							Opx	0.008	0.000	0.005					Act	0.0206	0.0000	0.0076

The analyses are normalized to fixed oxygen: phengite, O=11; biotite, O=11; amphibole, O=23; total cations without K=15; pyroxene, O=6, total cations=4. bdl, below detection limit. Mineral abbreviations follow Whitney & Evans (2010).

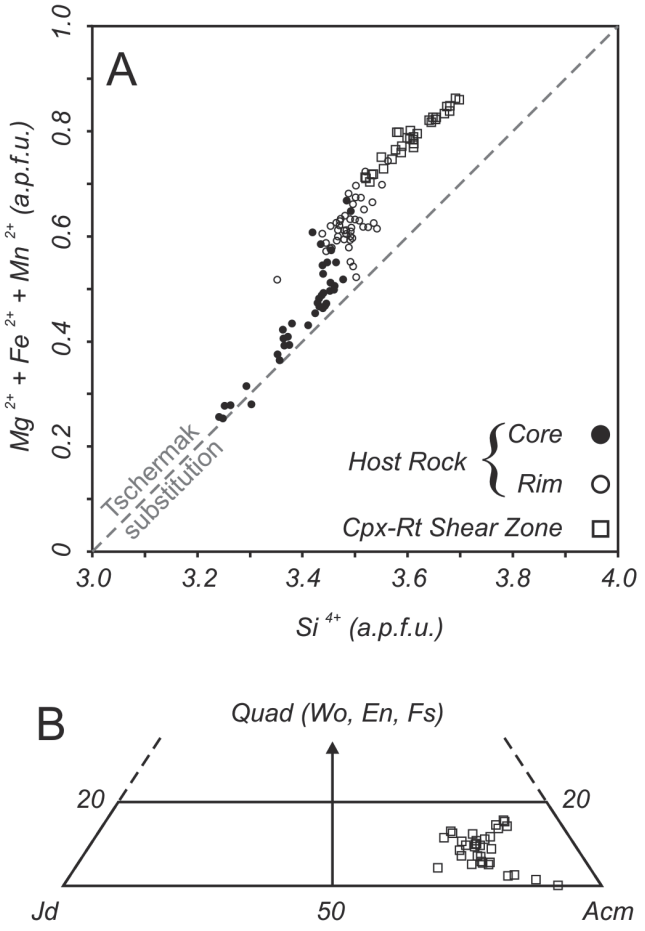

Fig. 5. (**a**) Si vs (Mg + Fe + Mn) diagram showing the phengite compositions both in the host rock and in the Cpx–Rt shear zone. Host rock analyses (rim + core) scatter along the muscovite–celadonite Tschermak substitution line (slope = 1) and range between 3.3 and 3.6 Si^{4+} a.p.f.u. whereas the Cpx–Rt shear zone analyses are clustered in the 3.6–3.7 range. (**b**) Quad–Jd–Acm diagram showing the Cpx chemical composition. Quad represents the Ca–Fe–Mg pyroxene vertex.

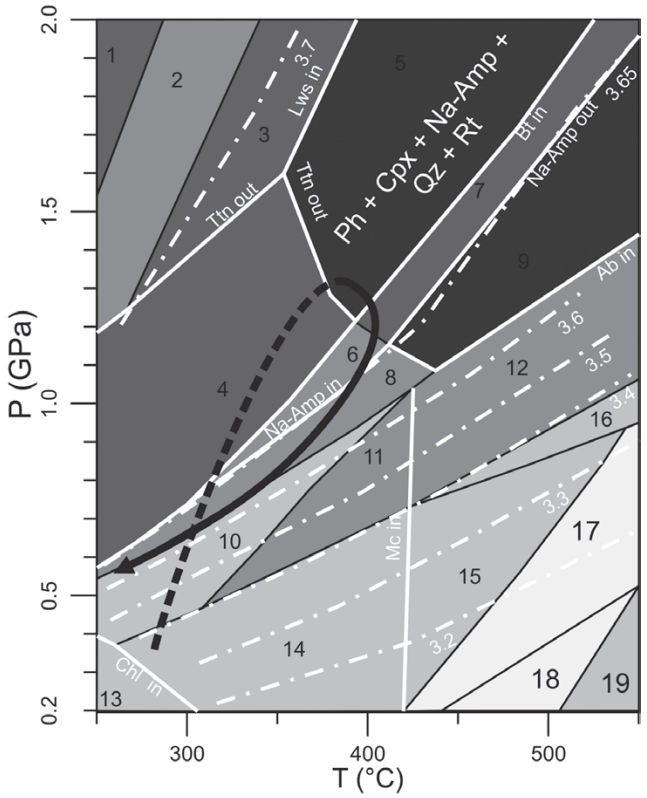

Fig. 6. *P–T* pseudosection in the NCKFMASHTO system as obtained with the Perple_X_07 software using a bulk composition of (wt %) Na_2O 0.82, CaO 0.53, K_2O 9.50, FeO_{Tot} 7.54, MgO 4.40, Al_2O_3 16.35, SiO_2 53.60, TiO_2 1.76 and O_2 0.30, with H_2O as saturated phase (mineral abbreviations after Whitney & Evans 2010). The continuous white lines indicate stability fields of the main phases; the white dot–dash lines are isopleths of the Si^{4+} a.p.f.u. content in Ph. It should be noted that highly substituted phengite compositions (i.e. 3.5–3.6 Si^{4+} a.p.f.u) are maintained to low-pressure conditions when rocks are exhumed along a cold path nearly parallel to the phengite isopleths. The inferred *P–T* path followed by the Variscan basement rocks during the Alpine reworking is also indicated (dashed and continuous bold black arrow). Field assemblages: 1, Chl Ph Cpx Lws Qz Rt; 2, Chl Ph Cpx Na-Amp Lws Qz Rt; 3, Ph Cpx Na-Amp Lws Qz Rt; 4, Ph Cpx Na-Amp Ttn Qz Rt; 5, Ph Cpx Na-Amp Qz Rt; 6, Bt Ph Cpx Na-Amp Ttn Qz Rt; 7, Bt Ph Cpx Na-Amp Qz Rt; 8, Bt Ph Cpx Ttn Ab Qz Rt; 9, Bt Ph Cpx Qz Rt; 10, Bt Ph Cpx Ttn Ab Mc Qz Rt; 11, Bt Ph Cpx Ab Mc Qz Rt; 12, Kfs Bt Ph Cpx Ab Qz Rt; 13, Bt Chl Ttn Ab Mc Qz Rt Hem; 14, Bt Ph Ttn Ab Mc Qz Rt Hem; 15, Kfs Bt Ph Ttn Ab Qz Rt Hem; 16, Kfs Bt Ph Cpx Ab Qz Rt Hem; 17, Kfs Bt Ep Ph Ab Qz Rt Hem Mag; 18, Kfs Bt Ph Ab Qz Rt Hem Mag; 19, Kfs Bt Ph Ab Qz Rt Mag.

bombs at *c*. 190 °C, and the other minerals in Savillex vials on a hotplate at around 100 °C. Chemical separation was performed with a two-stage anion exchange procedure using HBr for Pb and HNO_3 + HCl for U on AG 1-X8, 200–400 mesh resin. The samples were spiked with a ^{202}Pb–^{205}Pb–^{235}U spike. Other details of the procedure and measurement have been given by Corfu (2004). The decay constants are those of Jaffey *et al*. (1971). Plotting and regressions employed the program Isoplot of Ludwig (2003). Results are listed in Table 2 and shown in Figure 7.

Rt consists largely of tabular twinned prisms containing 5–15 ppm U and 0.3–4 ppm initial Pb. Cpx has mostly about 0.5 ppm U and half as much initial Pb. One fraction of Cpx was selected among grains full of Rt inclusions, the Cpx was dissolved at low temperature, and the residual Rt was recovered and dissolved separately. In this case the Cpx analysis yielded much higher U (11 ppm) and initial common Pb (5 ppm) contents; the liberated Rt consisted of very small and fragile pieces that could not be weighed. The data for all these minerals are all relatively unradiogenic, hence the age calculation is strongly dependent on the common Pb correction. The least radiogenic composition was found in the coatings of oxide or sulphide on Qz, although these values are clearly more radiogenic than normal crustal values ($^{206}Pb/^{204}Pb$ of 20.5). Such elevated initial values, however, are provided independently by regression lines through the various datasets. Use of the 3D concordia plot provides the means to deal with these types of data without exerting overstrong external controls by choosing specific compositions to correct the initial Pb (Fig. 7). The data define separate arrays for Rt (the low precision of this array reflecting the very small amount of Pb available for analysis) and the other minerals, although both lines are variously scattered. The intercepts with concordia, however, are similar, giving 53.7 ± 7.7 Ma for the Cpx–Ph–oxide regression and 48 ± 18 Ma for Rt (except for one of the Rt analyses, which plots very far from the line, but the significantly higher U content

Table 2. *U–Pb data for the acmite–rutile-bearing shear zone, sample T5A*

Properties	Weight (µg)	U (ppm)	Pbc (ppm)	Pbcom (pg)	238/204*	2σ%	206/204*	2σ%	235/204*	2σ%	207/204*	2σ%	238/206*	2σ%	207/206*	2σ%	204/206*	2σ%
R	5	15.19	0.31	3.5	3141	198	29	74	23	198	16.3	9.8	107	10	0.55773	0.30	0.03417	0.60
R	11	5.68	0.84	11	446	13	23.56	3.0	3.23	13	16.08	0.84	18.9	10	0.68267	0.15	0.04245	0.50
R	15	5.28	0.95	16	364.0	8.1	22.66	1.7	2.64	8.1	15.84	0.68	16.1	8	0.69928	0.30	0.04414	0.50
R	8	9.28	3.96	32	153.8	3.5	21.29	0.59	1.12	3.5	15.82	0.39	7.2	10	0.74277	0.15	0.04697	0.50
R	10	6.31	1.21	14	342.4	9.6	22.68	1.9	2.48	9.6	15.69	0.66	15.1	10	0.69204	0.17	0.04410	0.50
R incl in A				8	250	22	21.76	3.7	1.81	22	15.86	1.1	11.5	10	0.72866	0.15	0.04596	0.50
A with R incl	360	11.49	4.83	1663	156.06	0.48	21.578	0.31	1.132	0.48	15.79	0.38	7.2	1.0	0.73176	0.10	0.04634	0.40
A	2423	0.60	0.22	515	177.39	0.53	22.13	0.29	1.287	0.53	15.86	0.33	8.0	1.0	0.71675	0.11	0.04520	0.30
A fibrous	437	0.41	0.23	98	116.36	1.2	21.71	0.37	0.844	1.2	15.85	0.37	5.4	1.5	0.73018	0.20	0.04607	0.50
A blocky	2823	0.55	0.30	814	120	9	21.46	0.79	0.87	9.2	15.69	0.76	5.6	10	0.73118	0.30	0.04660	1.00
P				87	68.58	1.3	20.98	0.43	0.497	1.3	15.77	0.44	3.3	1.5	0.75147	0.15	0.04766	0.50
C				598905	0.078	0.61	20.518	0.20	0.001	0.61	15.774	0.30	0.00	1.0	0.76879	0.10	0.04874	0.10

R, rutile; A, acmite; P, phengite; C, oxide or sulphide coatings on quartz; incl, inclusions. Pbc, initial amount of common Pb. Pbcom, total amount of common Pb (initial + blank).
*Corrected for fractionation, spike and blank; error calculated by propagating the main sources of uncertainty.

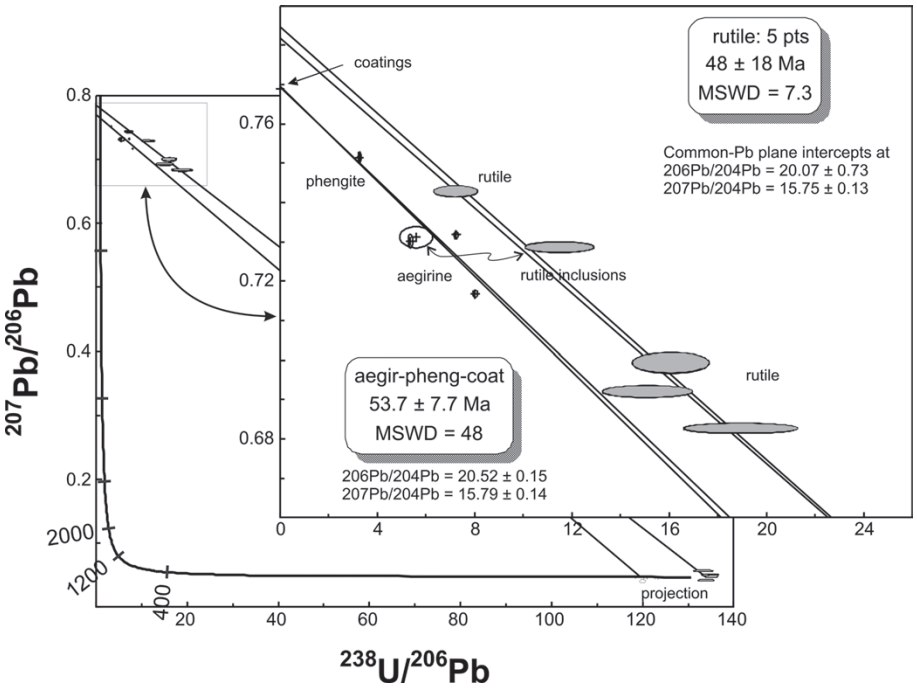

Fig. 7. TIMS U–Pb data showing a 3D concordia plot for the entire dataset. The data define separate arrays for Rt (its low precision reflecting the very small amount of Pb available for analysis) and the other minerals, although both lines are variously scattered. The intercepts with concordia, however, are similar. The age provided by Cpx–Ph and the coatings at 53.7 ± 7.7 Ma is considered the most reliable estimate for the age of shearing. The ellipses on the concordia curve (bottom right) are the calculated projections of the data points.

suggests that the fraction may have had inclusions of Zrn, which in this sample is very U-rich and discordant). The difference between the two arrays could be interpreted in two ways. One is that Rt formed after the Cpx, but that seems unlikely given their close paragenetic association. The alternative is that Rt remained open for the diffusion of Pb, or was affected by younger Pb loss that shifted the data towards younger ages. Interestingly, the very same age relationship is observed for the rutile inclusions liberated from the Cpx. In conclusion, the age provided by Cpx–Ph and the coatings at 53.7 ± 7.7 Ma is considered the most reliable estimate for development of these minerals.

Discussion

The new data integrating information on the fabrics and kinematics with geochronology and metamorphic petrology show that the Variscan basement along the East Tenda Shear Zone of Corsica underwent prograde high-pressure blueschist metamorphism in the Early Eocene (*c*. 50 Ma) during top-to-the-west-directed shearing. This shear sense is consistent with the kinematics of the Schistes Lustrés units overthrusting onto the European foreland (see Daniel *et al*. 1996; Molli & Malavieille 2010). Late reworking of the early-formed top-to-the-west ductile shear fabric by east-directed shear senses is also documented.

The Early Eocene timing of the Alpine peak metamorphism and the fabric-forming events reconstructed from the East Tenda Shear Zone confirms a Tertiary age for the Alpine metamorphism in Corsica. In particular, the U–Pb Rt ages presented herein are compatible with the maximum, discordant $^{40}Ar/^{39}Ar$ ages (46.6 ± 1.2 Ma) obtained from the East Tenda Shear Zone (Brunet *et al*. 2000), but older than the Late Eocene–Early Oligocene ages reported both from the East Tenda Shear Zone (Brunet *et al*. 2000) and the Schistes Lustrés nappe (Brunet *et al*. 2000; Martin *et al*. 2011). We emphasize here that the shape of the *P–T* path reconstructed for the

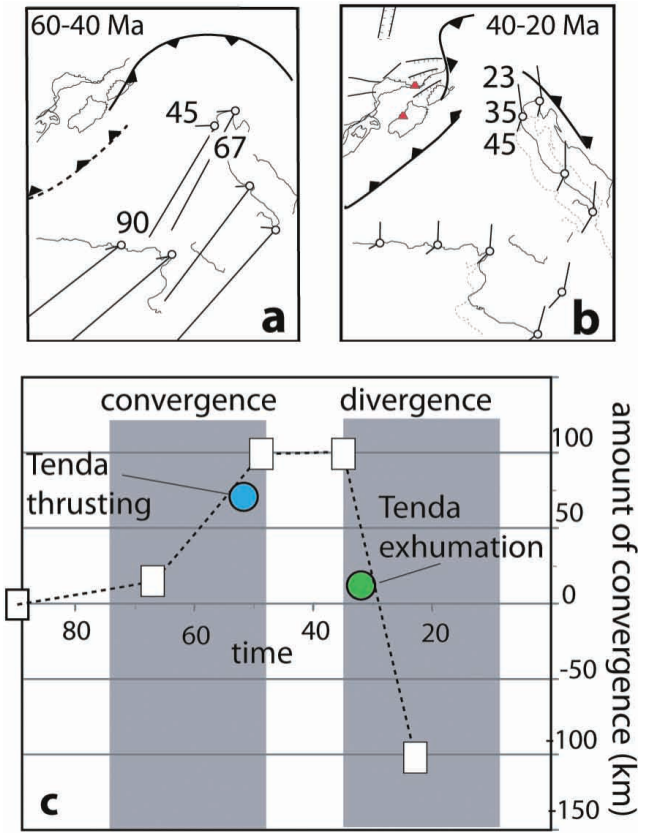

Fig. 8. Simplified palaeotectonic map of the central Mediterranean at (**a**) 60–40 Ma and (**b**) 40–20 Ma. The relative motion between Africa–Adria and Eurasia, from Dewey *et al*. (1989) rotation poles, is shown for reference points (white circle) with numbers referring to the age (Ma). Red triangles (dark grey in printed version) show calc-alkaline volcanoes, and the line indicates the main thrust fault (dashed if incipient). (**c**) Amount of net convergence or divergence (dashed line) expected along the East Tenda Shear Zone from the Dewey *et al*. (1989) rotation poles. The amount of trench rollback from 35 to 23 Ma is from Faccenna *et al*. (2001). Circles show the position of the Variscan basement rocks within the East Tenda Shear Zone considering that the Ligurian–Piedmontese overthrusting and subsequent extensional reactivation was accommodated along a 30°-dipping shear zone.

Cpx–Rt shear zone suggests that the ^{40}Ar–^{39}Ar phengite ages from the East Tenda Shear Zone probably record the continuous exhumation of this shear zone, as highly substituted phengite compositions persisted down to lower *P–T* conditions along a cooling–exhumation path (Fig. 6). This cooling–exhumation path can then provide a reason for the staircase geometry of the phengite argon release spectra obtained from the East Tenda Shear Zone samples (Brunet *et al*. 2000). A protracted history of deformation along this shear zone is also derived from stratigraphic data from the Alpine foreland (Egal 1992; Malasoma & Marroni 2007) and from the ^{40}Ar–^{39}Ar phengite ages (Brunet *et al*. 2000), which collectively document a Middle Eocene–Early Miocene timespan (see Molli *et al*. 2006). Consequently, a revised tectonic scenario is required to describe the polyphase deformation history along the East Tenda Shear Zone.

Assuming the East Tenda Shear Zone marks the major Alpine convergence boundary between the Ligurian–Piedmontese ocean and the Variscan Corsica, the activity of this shear zone can be framed within the Tertiary plate-tectonic framework of the central Mediterranean, estimating the expected convergence from plate kinematics reconstruction. To evaluate the relative motion between Adria and Eurasia, we adopt the Dewey *et al*. (1989) rotation pole for the Africa–Eurasia convergence and assume that the Adria motion was coherent with that of Africa (Van Der Voo 1993). The coherent motion of Adria with Africa during most of the Cenozoic is well established by palaeomagnetic data and palaeogeographical evidence (Channell *et al*. 1979; Muttoni *et al*. 2001). From this reconstruction it is possible to derive the direction and the amount of plate convergence expected along the main plate boundary in Corsica; that is, along the future East Tenda Shear Zone (Jolivet & Faccenna 2000; Piromallo & Faccenna 2004). We note that, for the time frame crucial for this tectonic reconstruction (Eocene), different velocity models converge towards the same solution (Savostin *et al*. 1986; Jolivet & Faccenna 2000; Rosenbaum *et al*. 2002; Capitanio & Goes 2006), which has been recently confirmed by new kinematic reconstructions (Cande & Stegman 2011).

The results are shown in Figure 8. Prior to 67 Ma, the convergence between Africa and Eurasia had a NE–SW trend, parallel to the East Tenda Shear Zone (Fig. 8a). In this scenario, the net convergence along the East Tenda Shear Zone was probably very minor, being dominated by a sinistral strike-slip component (Fig. 8c). Between *c*. 67 and *c*. 45 Ma, the motion changed sharply towards an east–west-striking convergence direction (Dewey *et al*. 1989; Jolivet & Faccenna 2000; Piromallo & Faccenna 2004). This significant kinematic change, well documented also in the recent kinematic model of Cande & Stegman (2011), probably had a profound influence on the tectonic evolution of the central Mediterranean and western Alps (Malusà *et al*. 2011). Decomposing the convergence vector into components parallel and perpendicular to the East Tenda Shear Zone, we expect a net convergence perpendicular to the East Tenda Shear Zone of about 80–90 km and a right lateral strike-slip component of the order of *c*. 40–50 km (Fig. 8c). From *c*. 45 to *c*. 30–35 Ma, the plate convergence was NNE–SSW directed, and hence parallel to the East Tenda Shear Zone, probably producing significant left-lateral deformation (Fig. 8b). At *c*. 30–35 Ma, the dynamics of the system again changed and the roll-back of the Apennines subduction system commenced. Rifting in the Provençal–Ligurian basin started during the latest Eocene–Early Oligocene (34–28 Ma) and ended in Aquitanian (21 Ma) (Séranne 1999). Subsequently, the central oceanic portion of the basin was generated between the late Aquitanian and late Burdigalian (21–16 Ma), associated with the counterclockwise rotation of the Corsica–Sardinia Block (Speranza *et al*. 2002) and the onset of the Tyrrhenian back-arc extension (Jolivet *et al*. 1998). The East Tenda Shear Zone therefore may have been active as a major thrust in the period from *c*. 67 to 40–45 Ma. It is expected to have been subsequently reactivated as an extensional shear zone at *c*. 30–20 Ma when the high-pressure core of the Alpine orogen in Corsica was finally exhumed during post-orogenic extension (Jolivet *et al*. 1990).

The Early Eocene timing of the Alpine peak metamorphism and the fabric-forming events in the East Tenda Shear Zone reconstructed in this study imply that net convergence in Corsica may have lasted slightly more than 20 Ma (between *ca*. 67 and 45–40 Ma; Early–Middle Eocene), and that a large part of the expected 80–90 km of shortening was mostly accommodated along the East Tenda Shear Zone to produce underthrusting of the Variscan basement to a minimum depth of *c*. 40 km (assuming an average density for the basement rocks of 2800 kg m^{-3}) along a 30°-dipping thrust zone (Fig. 8c). This pulse of convergence was probably mostly accommodated along the former continent–ocean transition zone (Vitale Brovarone *et al*. 2011*b*) with final shear strain localization along the East Tenda Shear Zone. This process caused the compressional reactivation of the former continental passive margin, which resulted in overthrusting of the

subducted tracts of the Ligurian–Piedmontese Ocean onto the Variscan Corsica. The recent zircon U–Pb dating of eclogitic metamorphism in continental-derived slivers embedded within the Schistes Lustrés nappe (Martin *et al*. 2011) suggests that convergence and related subduction metamorphism affected the Ligurian–Piedmontese oceanic up to Late Eocene time. This long-lasting compressional tectonism is also recorded by post-37 Ma thrusting in the Alpine foreland of Corsica (Egal 1992; Brunet *et al*. 2000; Malasoma & Marroni 2007), which also suggests that East Tenda Shear Zone rocks were exhumed and entered brittle deformation environments at that time.

In the timespan relevant for this study (Eocene), correlation with the tectono-metamorphic evolution of the Western Alps may contribute to elucidate the sequence of deformation events along the Corsica–Europe active margin of the Alpine chain. In particular, two points deserve consideration. First, the main phase of exhumation of the Schistes Lustrés accretionary complex in the Western Alps (Agard *et al*. 2002) occurred concurrently with the Early Eocene climax of Alpine metamorphism in the Variscan basement of Corsica documented in this study. Second, as for Alpine Corsica (see Martin *et al*. 2011), the climax of subduction-zone metamorphism in the Western Alps occurred later, during the Middle–Late Eocene (from *c*. 45 to 35 Ma; e.g. Rubatto & Hermann 2003; Meffan-Main *et al*. 2004; Di Vincenzo *et al*. 2006; Malusà *et al*. 2011), in a scenario there dominated by the continuous subduction of the European margin and collision with the Adria plate (see Schmid *et al*. 1996). A polyphase evolution can be thus envisaged: (1) the Alpine activation of the East Tenda Shear Zone within the Variscan basement of Corsica occurred synchronously with exhumation of the oceanic-derived Schistes Lustrés accretionary complex, and the East Tenda Shear Zone may be thus interpreted as the basal thrust of the early structured Schistes Lustrés accretionary complex; (2) shortly after achievement of the Alpine metamorphic climax (Middle–Late Eocene), exhumation of the high-pressure core of the orogen occurred; Corsica was disconnected from the Alpine system and incorporated in the back-arc domain of the Apennine subduction system, which accommodated the overall plate convergence at least from the Late Eocene onward (e.g. Faccenna *et al*. 2001; Lustrino *et al*. 2009). This evolutionary scenario requires an along-strike space–time transition in the mode and regimes of oceanic subduction along the Alpine–Apennine junction (see, e.g. Vignaroli *et al*. 2008; Argnani 2010).

Conclusion

The finding of a clinopyroxene–rutile-bearing shear zone within the East Tenda Shear Zone and definition of its *P–T–t* evolution provide new constraints on the metamorphic regimes and timing of the Alpine reworking of the Variscan crust in Corsica. We document an Early Eocene phase of orogenic construction that can be linked to the general scenario of plate convergence in the central Mediterranean during the Palaeogene. Evidence is provided for a polyphase evolution of the East Tenda Shear Zone, which was first activated as a major thrust to exhume the fossil Schistes Lustrés accretionary complex of the Western Alps during the Eocene and then reactivated as an extensional shear zone in Oligocene–Miocene times at the back of the eastward retreating Apennine subduction system.

We are indebted to L. Jolivet for having introduced us to the geology of the Alpine Corsica. This paper benefited from discussions on themes dealing with the Alpine geology of Corsica held with J. Malavieille, G. Molli and A. Vitale Bravarone, and during the CorseAlp2011 meeting. We also acknowledge advice from and discussion with H. J. Massone. This paper benefited from constructive criticism and advice from three anonymous reviewers. Part of the research was funded by grants provided by the GeoQuTe Lab coordinated by F. Salvini.

References

Agard, P., Monié, P., Jolivet, L. & Goffé, B. 2002. Exhumation of the Schistes Lustrés complex: in situ laser probe $^{40}Ar/^{39}Ar$ constraints and implications for the Western Alps. *Journal of Metamorphic Geology*, **20**, 599–618, doi:10.1046/j.1525-1314.2002.00391.x.

Amaudric Du Chaffaut, S. & Saliot, P. 1979. La région de Corte: secteur-clé pour la compréhension du métamorphisme alpine en Corse. *Bulletin de la Société Géologique de France*, **21**, 149–154.

Argnani, A. 2010. Plate tectonics and the boundary between Alps and Apennines. *Bollettino della Società Geologica Italiana*, **128**, 317–330.

Austrheim, H. 1987. Eclogitization of lower crustal granulites by fluid migration through shear zones. *Earth and Planetary Science Letters*, **81**, 221–232.

Bezert, P. & Caby, R. 1988. Sur l'âge post-bartonien des événements tectono-métamorphiques alpins en bordure orientale de la Corse cristalline. *Bulletin de la Société Géologique de France*, **8**, 965–971.

Brunet, C., Monié, P., Jolivet, L. & Cadet, J.P. 2000. Migration of compression to extension in the Tyrrhenian Sea, insight from $^{40}Ar/^{39}Ar$ ages on micas along a transect form Corsica to Tuscany. *Tectonophysics*, **321**, 127–155.

Cande, S.C. & Stegman, D.R. 2011. Indian and African plate motions driven by the push force of the Réunion plume head. *Nature*, **475**, 47–51.

Capitanio, F.A. & Goes, S. 2006. Mesozoic spreading kinematics: consequences for Cenozoic Central and Western Mediterranean subduction. *Geophysical Journal International*, **165**, 804–816, doi:10.1111/j.1365-246X.2006.02892.x.

Caron, J.M., Kienast, J.R. & Triboulet, C. 1981. High-pressure–low-temperature metamorphism and polyphase Alpine deformation at Sant'Andrea di Cotone (Eastern Corsica, France). *Tectonophysics*, **78**, 419–451.

Channell, J.E.T., D'Argenio, B. & Horvath, F. 1979. Adria, the African promontory, in Mesozoic Mediterranean palaeogeography. *Earth-Science Reviews*, **15**, 213–292.

Chopin, C., Beyssac, O., Bernard, S. & Malavielle, J. 2008. Aragonite–grossular intergrowths in eclogite-facies marble, Alpine Corsica. *European Journal of Mineralogy*, **20**, 857–865.

Clark, C., Mumm, A.S. & Faure, K. 2005. Timing and nature of fluid flow and alteration during Mesoproterozoic shear zone formation, Olary Domain, South Australia. *Journal of Metamorphic Geology*, **23**, 147–164, doi: 10.1111/j.1525-1314.2005.00568.

Cohen, C.R., Schweickert, R.A. & Odom, A.L. 1981. Age of emplacement of the Schistes Lustrés nappe, Alpine Corsica. *Tectonophysics*, **73**, 267–283.

Connolly, J.A.D. 2005. Computation of phase equilibria by linear programming: a tool for geodynamic modelling and its application to subduction zone decarbonation. *Earth and Planetary Science Letters*, **236**, 524–541.

Corfu, F. 2004. U–Pb age, setting, and tectonic significance of the anorthosite–mangerite–charnockite–granite suite, Lofoten–Vesterålen, Norway. *Journal of Petrology*, **45**, 1799–1819.

Dallan, L. & Nardi, R. 1984. Ipotesi sulla evoluzione dei domini 'Liguri' della Corsica nel quadro della paleogeografia e della paleottetonica delle unità alpine. *Bollettino della Società Geologica Italiana*, **103**, 517–527.

Dallan, L. & Puccinelli, A. 1995. Geologia della regione tra Bastia e St-Florent (Corsica Settentrionale). *Bollettino della Società Geologica Italiana*, **114**, 23–66.

Daniel, J.M., Jolivet, L., Goffe, B. & Poinssot, C. 1996. Crustal-scale strain partitioning: footwall deformation below the Alpine Oligo-Miocene detachment of Corsica. *Journal of Structural Geology*, **18**, 41–59.

Dewey, J.F., Helman, M.L., Turco, E., Hutton, D.H.W. & Knott, S.D. 1989. Kinematics of the western Mediterranean. *In*: Coward, M.P., Dietrich, D. & Park, R.G. (eds) *Alpine Tectonics*. Geological Society, London, Special Publications, **45**, 265–283.

Dipple, G.M. & Ferry, J.M. 1992. Metasomatism and fluid flow in ductile fault zones. *Contributions to Mineralogy and Petrology*, **112**, 149–164.

Di Vincenzo, G., Tonarini, S., Lombardo, B., Castelli, D. & Ottolini, L. 2006. Comparison of $^{40}Ar–^{39}Ar$ and Rb–Sr data on phengites from the UHP Brossasco–Isasca Unit (Dora Maira Massif, Italy): implications for dating white mica. *Journal of Petrology*, **47**, 1439–1465, doi:10.1093/petrology/egl018.

Durand-Delga, M. 1984. Principaux traits de la Corse Alpine et correlations avec les Alpes Ligures. *Memorie della Società Geologica Italiana*, **28**, 285–329.

Egal, E. 1992. Structures and tectonic evolution of the external zone of Alpine Corsica. *Journal of Structural Geology*, **14**, 1215–1228.

Essene, E. 1968. Relatively pure jadeite from a siliceous Corsican gneiss. *Earth and Planetary Science Letters*, **5**, 270–272.

Faccenna, C., Becker, T.W., Lucente, F.P., Jolivet, L. & Rossetti, F. 2001. History of subduction and back-arc extension in the Central Mediterranean. *Geophysical Journal International*, **145**, 809–820.

Fournier, M., Jolivet, L., Goffé, B. & Dubois, R. 1991. The Alpine Corsica metamorphic core complex. *Tectonics*, **10**, 1173–1186.

Gibbons, W. & Horak, J. 1984. Alpine metamorphism of Hercynian hornblende granodiorite beneath the blueschist facies Schistes Lustrés nappe of NE Corsica. *Journal of Metamorphic Geology*, **2**, 95–113.

Gueydan, F., Leroy, Y.M., Jolivet, L. & Agard, P. 2003. Analysis of continental midcrustal strain localization induced by microfracturing and reaction-softening. *Journal of Geophysical Research*, **108**, doi:10.1029/JB000611.

Holland, T.J.B. & Powell, R. 1998. An internally consistent thermodynamic data set for phases of petrological interest. *Journal of Metamorphic Geology*, **16**, 309–343.

Imber, J., Holdsworth, R.E., Butler, C.A. & Lloyd, G.E. 1997. Fault-zone weakening processes along the reactivated Outer Hebrides Fault zone, Scotland. *Journal of the Geological Society, London*, **154**, 105–109.

Jaffey, A.H., Flynn, K.F., Glendenin, L.E., Bentley, W.C. & Essling, A.M. 1971. Precision measurement of half-lives and specific activities of ^{235}U and ^{238}U. *Physical Review, Section C, Nuclear Physics*, **4**, 1889–1906.

John, T., Medvedev, S., Rüpke, L.H., Andersen, T.B., Podladchikov, Y.Y. & Austrheim, H.O. 2009. Generation of intermediate-depth earthquakes by self-localizing thermal runaway. *Nature Geoscience*, **2**, 137–140.

Jolivet, L. & Faccenna, C. 2000. Mediterranean extension and the Africa–Eurasia collision. *Tectonics*, **19**, 1095–1106.

Jolivet, L., Dubois, R., Fournier, M., Goffé, B., Michard, A. & Jourdan, C. 1990. Ductile extension in Alpine Corsica. *Geology*, **18**, 1007–1010.

Jolivet, L., Faccenna, C., *et al.* 1998. Midcrustal shear zones in postorogenic extension: example from the Northern Tyrrhenian Sea. *Journal of Geophysical Research*, **103**, 12123–12160.

Jolivet, L., Raimbourg, H., Labrousse, L., Avigad, D., Leroy, Y., Austrheim, H. & Andersen, T.B. 2005. Softening triggered by eclogitization, the first step toward exhumation during continental subduction. *Earth and Planetary Science Letters*, **237**, 532–547.

Labrousse, L., Hetény, G., Raimbourg, H., Jolivet, L. & Andersen, T.B. 2010. Initiation of crustal-scale thrusts triggered by metamorphic reactions at depth: insights from a comparison between the Himalayas and the Scandinavian Caledonides. *Tectonics*, **29**, doi:10.1029/2009TC002602.

Lahondère, D. & Guerrot, C. 1997. Sm–Nd dating of Alpine eclogitic metamorphism in Corsica: evidence for Late Cretaceous subduction beneath the Corsican–Sardinian block. *Géologie de la France*, **3**, 3–11.

Ludwig, K.R. 2003. *Isoplot 3.0. A Geochronological Toolkit for Microsoft Excel.* Berkeley Geochronology Center, Special Publications, **4**.

Lustrino, M., Morra, V., Fedele, L. & Franciosi, L. 2009. Beginning of the Apennine subduction system in central western Mediterranean: constraints from Cenozoic 'orogenic' magmatic activity of Sardinia (Italy). *Tectonics*, **28**, doi:10.1029/2008TC002419.

Malasoma, A. & Marroni, M. 2007. HP/LT metamorphism in the Volparone Breccia (Northern Corsica, France): evidence for involvement of the Europe/Corsica continental margin in the Alpine subdution zone. *Journal of Metamorphic Geology*, **25**, 529–545.

Malavieille, J., Chemenda, A. & Larroque, C. 1998. Evolutionary model for Alpine Corsica: mechanism for ophiolite emplacement and exhumation of high-pressure rocks. *Terra Nova*, **10**, 317–322.

Malusà, M., Faccenna, C., Garzanti, E. & Polino, R. 2011. Divergence in subduction zones and exhumation of high pressure rocks (Eocene Western Alps). *Earth and Planetary Science Letters*, **310**, 21–32.

Maluski, H. 1977. Application de la méthode $^{40}Ar/^{39}Ar$ aux minéraux des roches cristallines perturbées par les événements thermiques et tectoniques en Corse. *Bulletin de la Société Géologique de France*, **19**, 849–850.

Martin, L.A.J., Rubatto, D., Vitale Brovarone, A. & Hermann, J. 2011. Late Eocene lawsonite-eclogite facies metasomatism of a granulite sliver associated to ophiolites in Alpine Corsica. *Lithos*, **125**, 620–640, doi:10.1016/j.lithos.2011.03.015.

Massonne, H.J. & Willner, A.P. 2008. Phase relations and dehydration behaviour of psammopelite and mid-ocean ridge basalt at very-low-grade to low-grade metamorphic conditions. *European Journal of Mineralogy*, **20**, 867–879.

Mattauer, M., Faure, M. & Malavieille, J. 1981. Transverse lineation and large scale structures related to Alpine obduction in Corsica. *Journal of Structural Geology*, **3**, 401–409.

Meffan-Main, F., Cliff, R.A., Barnicoat, A.C., Lombardo, B. & Compagnoni, R. 2004. A Tertiary age for Alpine metamorphism in the Gran Paradiso massif, western Alps: a Rb–Sr microsampling study. *Journal of Metamorphic Geology*, **22**, 267–281.

Molli, G. & Malavieille, J. 2010. Orogenic processes and the Corsica/Apennines geodynamic evolution: insights from Taiwan. *International Journal of Earth Sciences*, **100**, 1207–1224, doi:10.1007/s00531-010-0598-y.

Molli, G., Tribuzio, R. & Marquer, D. 2006. Deformation and metamorphism at the eastern border of the Tenda Massif (NE Corsica): a record of subduction and exhumation of continental crust. *Journal of Structural Geology*, **28**, 1748–1766.

Muttoni, G., Garzanti, E., Alfonsi, L., Cirilli, S., Germani, D. & Lowrie, W. 2001. Motion of Africa and Adria since the Permian: paleomagnetic and paleoclimatic constraints from northern Libya. *Earth and Planetary Science Letters*, **192**, 159–174.

Piromallo, C. & Faccenna, C. 2004. How deep can we find the traces of Alpine subduction? *Geophysical Research Letters*, **31**, doi:10.1029/2003GL019288.

Ravna, E.J.K., Andersen, T.B., Jolivet, L. & De Capitani, C. 2010. Cold subduction and the formation of lawsonite eclogite–constraints from prograde evolution of eclogitized pillow lava from Corsica. *Journal of Metamorphic Geology*, **28**, 381–395, doi:10.1111/j.1525-1314.2010.00870.x.

Rosenbaum, G., Lister, G.S. & Duboz, C. 2002. Relative motions of Africa, Iberia and Europe during Alpine orogeny. *Tectonophysics*, **359**, 117–129.

Rossi, P.H., Durand-Delga, M., Lahondère, J.C. & Lahondère, D. 2003. *Carte géologique de la France à 1/50.000, feuille Santo Pietro di Tenda*. BRGM, Orleans.

Rubatto, D. & Hermann, J. 2003. Zircon formation during fluid circulation in eclogites (Monviso, Western Alps): implications for Zr and Hf budget in subduction zones. *Geochimica et Cosmochimica Acta*, **67**, 2173–2187.

Savostin, L.A., Sibuet, J.-C., Zonenshain, L.P., Le Pichon, X. & Roulet, M.-J. 1986. Kinematic evolution of the Tethys Belt from the Atlantic Ocean to the Pamirs since the Triassic. *Tectonophysics*, **123**, 1–35.

Schmid, S.M., Pfiffner, O.A., Froitzheim, N., Schönborn, G. & Kissling, E. 1996. Geophysical–geological transect and tectonic evolution of the Swiss–Italian Alps. *Tectonics*, **15**, 1036–1064.

Selverstone, J., Morteani, G. & Staude, J.-M. 1991. Fluid channeling during ductile shearing: transformation of granodiorite into aluminous schist in the Tauern Window, Eastern Alps. *Journal of Metamorphic Geology*, **9**, 419–431.

Séranne, M. 1999. The Gulf of Lion continental margin (NW Mediterranean) revisited by IBS: an overview. *In*: Durand, B., Jolivet, L., Horváth, F. & Séranne, M. (eds) *The Mediterranean Basins: Tertiary Extension within the Alpine Orogen*. Geological Society, London, Special Publications, **156**, 15–36.

Speranza, F., Villa, I.M., Sagnotti, L., Florindo, F., Cosentino, D., Cipollati, P. & Mattei, M. 2002. Age of the Corsica–Sardinia rotation and Ligure–Provençal Basin spreading: new paleomagnetic and Ar/Ar evidence. *Tectonophysics*, **347**, 231–251.

Tribuzio, R. & Giacomini, F. 2002. Blueschist facies metamorphism of peralkaline rhyolites from the Tenda crystalline massif (northern Corsica): evidence for involvement in the Alpine subduction event? *Journal of Metamorphic Geology*, **20**, 513–526.

Van Der Voo, R. 1993. *Paleomagnetism of the Atlantic, Tethys and Iapetus Oceans*. Cambridge University Press, Cambridge.

Vignaroli, G., Faccenna, C., Jolivet, L., Piromallo, C. & Rossetti, F. 2008. Subduction polarity reversal at the junction between the Western Alps and the Northern Apennines, Italy. *Tectonophysics*, **450**, 34–50.

Vitale Brovarone, A., Beltrando, M., *et al.* 2011*a*. Inherited ocean–continent transition zones in deeply subducted terranes: insights from Alpine Corsica. *Lithos*, **124**, 273–290, doi:10.1016/j.lithos.2011.02.013.

Vitale Brovarone, A., Groppo, C., Hetényi, G., Compagnoni, R. & Malavieille, J. 2011*b*. Coexistence of lawsonite-bearing eclogite and blueschist: phase equilibria modelling of Alpine Corsica metabasalts and petrological evolution of subducting slabs. *Journal of Metamorphic Geology*, **29**, 583–600, doi:10.1111/j.1525-1314.2011.00931.x.

Waters, C.N. 1990. The Cenozoic tectonic evolution of Alpine Corsica. *Journal of the Geological Society, London*, **147**, 811–824.

Whitney, D.L. & Evans, B. 2010. Abbreviations for names of rock-forming minerals. *American Mineralogist*, **95**, 185–187.

Received 10 October 2011; revised typescript accepted 4 June 2012.
Scientific editing by Robert Anczkiewicz.